

Electronic Supplementary Information (ESI) for

**Sensitized triplet-triplet annihilation upconversion in water
and its application to photochemical transformations**

Christoph Kerzig* and Oliver S. Wenger*

Contents

1	General experimental details	S1
2	Synthetic procedures and characterization data	S3
3	Rate constant determinations	S6
	3.1 Triplet-triplet energy transfer	S6
	3.2 Triplet-triplet annihilation	S6
4	Control experiments with anthracene-9-propionate APA	S7
5	Upconversion quantum yield estimation	S9
6	Applicability of the new dyads as oxygen probes	S10
7	Monodechlorination of trichloroacetate TCA ⁻	S12
8	Supplementary references	S18

1 General experimental details

All chemicals for optical spectroscopy and irradiation experiments were obtained commercially in the highest available purity and used as received (rutheniumtris(bipyridine) dichloride hexahydrate, 99.95 %, Aldrich; rutheniumtris(phenanthroline) dichloride hydrate, 98 %, Aldrich; pyrene-1-carboxylic acid, 97 %, Aldrich; anthracene-9-carboxylic acid, 99 %, Aldrich; anthracene-9-propionic acid, 96 %, Alfa Aesar; 9-(methylaminomethyl)anthracene, 99 %, Aldrich; sodium trichloroacetate, 97 %, Acros; triethanolamine, > 99 %, Aldrich; sodium hydrogen phosphate, > 99 %, Aldrich; sodium dihydrogen phosphate, > 99 %, Aldrich). The solvent (except for the syntheses presented in Section 2 of the ESI) was ultrapure Millipor MilliQ water (specific resistance, 18.2 MΩ cm). Unless otherwise indicated, the solutions

were purged with argon (4.8, PanGas) for ten minutes before the measurements and sealed under argon (1 atm) using cuvettes with septum caps. Experiments on air-saturated solutions (*i.e.*, aerated solutions) were carried out with freshly prepared aqueous solutions without additional air-purging. To ensure both fast dissolution of the neutral anthracene derivatives and their dissociation into ionic forms in aqueous solution, the pH of the solvent was either adjusted to 2–3 (**MAMA**) or to 11–12.2 (**ACA** and **APA**). Hydrochloric acid (37 %, VWR) and sodium hydroxide (98 %, Acros) were used for that purpose.

All steady-state absorption and luminescence spectra were recorded using a Cary 5000 spectrophotometer (Varian) and a Fluorolog-3-22 instrument (Horiba Jobin-Yvon), respectively.

The solutions used for luminescence spectroscopy were strongly diluted to avoid filter effects; absorptions at the excitation wavelength as well as in the luminescence/absorption overlap area were smaller than 0.1. All emission spectra were corrected for the wavelength-dependent sensitivity of the spectrometer.

Emission quantum yields were determined against anthracene-9-carboxylate^{1,2} or rutheniumtris(bipyridine)³ as standards. All quantum yield determinations were carried out at two different excitation wavelengths (with a double determination at each wavelength). The maximum relative deviation from the average value did not exceed 3 %. For the measurements of the upconversion power dependencies (Fig. 5 (c) of the main paper) the Fluorolog-3-22 was equipped with a 532 nm (optical output, up to 500 mW) DPSS cw laser (Roithner Lasertechnik) as light source with precisely adjustable radiative power and high output stability (< 1 %). The modular construction of the Fluorolog-3-22 allowed both a straightforward connection of this laser and blocking of the internal light source. In the luminescence detection window, the collimated beam diameter of the laser was 3 mm.

Fluorescence lifetime and quenching measurements with the anthracenes were performed on a LifeSpec II spectrometer (time-correlated single photon counting technique) from Edinburgh Instruments using picosecond pulsed diode lasers for excitation at 375 nm or 405 nm. Unquenched lifetimes of excited singlet states were measured with solutions containing very low fluorophore concentrations (30 ... 50 μ M) to avoid self-quenching.

An LP920-KS apparatus from Edinburgh Instruments was employed for UV-Vis transient absorption and emission spectroscopy. Excitation was performed by a frequency-doubled Nd:YAG laser (Quantel Brilliant b, *ca.* 10 ns pulse width). The excitation intensities (from 7 to 65 mJ per pulse) were varied by the Q-switch delays and measured with a pyroelectric detector. A beam expander (GBE02-A from Thorlabs) was used to ensure homogeneous excitation (beam diameter in front of the cuvette window, 1.3 cm) in the detection volume thus allowing the precise determination of excited-state concentrations in the cuvette as well as the analysis of second-order kinetics. Detection of transient absorption spectra occurred on an iCCD camera (Andor), whereas kinetics at a single wavelength were recorded using a photomultiplier tube.

All spectroscopic experiments were carried out at room temperature (293 K).

2 Synthetic procedures and characterization data

Commercially available solvents, starting materials and reagents were used as received. All synthetic steps were carried out under a nitrogen atmosphere. Solutions of the target complexes were protected from light (during synthesis and purification), and the isolated products were stored in the dark.

¹H NMR spectra were measured at 295 K on a Bruker Avance III spectrometer operating at a frequency of 400 MHz. Chemical shifts were referenced to the solvent peaks⁴. Thin layer chromatography was carried out using TLC Silica gel 60 F₂₅₄ plates from Merck. ESI mass spectra were recorded on a Di-ESI-MS 8030 Plus instrument (Shimadzu). High resolution mass spectra were measured on a Bruker maXis 4G QTOF ESI spectrometer by Dr. Heinz Nadig. Ms. Sylvie Mittelheisser carried out elemental analysis on a Vario Micro Cube instrument.

Photochemical characterization data are presented in the main paper.

cis-Bis(1,10-phenanthroline)dichlororuthenium(II) dihydrate, *cis*-[Ru(phen)₂Cl₂]·2 H₂O

The dyad precursor *cis*-[Ru(phen)₂Cl₂]·2H₂O was prepared according to a combination of literature procedures⁵⁻⁷ starting from a mixture of RuCl₃·4 H₂O (2.50 g, 8.94 mM), 1,10-phenanthroline monohydrate (3.73 g, 18.78 mmol) and LiCl (2.52 g) in DMF (30 mL). The crude product (4.1 g), which was isolated as reported in ref. ⁵, was washed with water (3 × 25 mL) and freshly distilled diethyl ether (2 × 20 mL). Since the ¹H NMR spectrum of the black solid still revealed substantial impurities (not identified), further purification steps^{6,7} were carried out. First, the black solid was washed with aqueous LiCl solution (10 %, 15 mL), water (2 × 20 mL), acetone (2 × 20 mL) and diethyl ether (20 mL). Second, remaining impurities were removed by suspending the product in hot methanol (150 mL), followed by filtration and washing the black solid with acetone (3 × 15 mL). The product was dried under reduced pressure to afford *cis*-[Ru(phen)₂Cl₂]·2 H₂O (2.3 g, 45 %).

The recorded ¹H NMR spectrum (400 MHz, DMSO-*d*₆) is completely identical with that reported in the literature⁶.

4-Methyl-4'-(2-hydroxyethylpyrenyl)-2,2'-bipyridine, (bpy-pyrene)

The ligand **bpy-pyrene** was prepared from 4,4'-dimethyl-2,2'-bipyridine (2.00 g, 10.9 mmol) and 1-pyrenecarboxyaldehyde (2.75 g, 11.9 mmol) in THF (≥ 99.9 %, inhibitor-free, Aldrich) following the procedure previously reported by Castellano *et al.*⁸. Contrary to that method, LDA was not prepared *in situ* but added directly via cannula (6 mL of a 2.0 M LDA solution in THF/heptane/ethylbenzene as obtained from Aldrich). The crude product (4.1 g) was recrystallized from 40 mL of hot CHCl₃ to yield

bpy-pyrene (2.7 g, 60 %) as a white solid.

¹H NMR data (400 MHz, CDCl₃) are in agreement with those presented in ref. ⁸.

Bis(2,2'-bipyridine)[4-methyl-4'-(2-hydroxyethylpyrenyl)-2,2'-bipyridine]ruthenium(II) hexafluorophosphate, [Ru(bpy)₂(bpy-pyrene)](PF₆)₂ (RuPy1)

A deep violet suspension of *cis*-bis(2,2'-bipyridine)dichlororuthenium(II) dihydrate (0.30 g, 0.58 mmol, Alfa Aesar) and **bpy-pyrene** (0.26 g, 0.63 mmol) in methanol (60 mL) was heated at reflux for 5 hours. The hot reaction mixture was filtered, and then the filtrate was allowed to cool to room temperature. After the addition of water (20 mL) to the deep orange solution, saturated aqueous KPF₆ (20 mL) was added dropwise, generating an orange precipitate of the target complex as its hexafluorophosphate salt. After storing the mixture in the fridge overnight, the precipitate was filtered and washed with cold water (3 × 20 mL) and subsequently with freshly distilled diethyl ether (20 mL). The solid was dried at room temperature in the dark to yield the crude product (0.4 g). Final purification was carried out by double recrystallization from ethanol (99 %) to afford **RuPy1** (0.096 g, 15 %) as an orange-red solid.

R_f = 0.48 (CH₃CN/H₂O/sat. aqueous KNO₃ 100:10:1).

MS (ESI): *m/z* 973 [M–PF₆]⁺, 414 [M–2PF₆]²⁺.

HRMS: Calcd. for C₄₉H₃₈N₆ORu ([M–2PF₆]²⁺): *m/z* 414.1076, found: *m/z* 414.1079.

Elemental analysis: Anal. calcd. for C₄₉H₃₈F₁₂N₆OP₂Ru·1.0 H₂O (%): C 51.81, H 3.55, N 7.40; found: C 52.05, H 3.94, N 7.39.

¹H NMR (400 MHz, ACN-*d*₃): δ [ppm] 8.50-8.40 (5H), 8.31-8.24 (2H), 8.19-7.88 (12H), 7.70-7.54 (4H), 7.48-7.26 (6H), 7.19-7.08 (2H), 6.19-6.10 (1H), 3.94-3.90 (1H), 3.50-3.41 (2H), 2.41-2.32 (3H).

Bis(1,10-phenanthroline)[4-methyl-4'-(2-hydroxyethylpyrenyl)-2,2'-bipyridine]ruthenium(II) hexafluorophosphate, [Ru(phen)₂(bpy-pyrene)](PF₆)₂ (RuPy2)

RuPy2 was prepared from *cis*-[Ru(phen)₂Cl₂]₂·2H₂O (0.30 g, 0.53 mmol) and **bpy-pyrene** (0.24 g, 0.58 mmol). Synthesis and purification were carried out according to the above mentioned procedure for the preparation of **RuPy1**. Finally, the PF₆[−] salt of **RuPy2** (0.078 g, 13 %) was isolated as an orange solid.

R_f = 0.52 (CH₃CN/H₂O/sat. aqueous KNO₃ 100:10:1).

MS (ESI): *m/z* 1021 [M–PF₆]⁺, 438 [M–2PF₆]²⁺.

HRMS: Calcd. for C₅₃H₃₈N₆ORu ([M–2PF₆]²⁺): *m/z* 438.1077, found: *m/z* 438.1082.

Elemental analysis: Anal. calcd. for C₅₃H₃₈F₁₂N₆OP₂Ru·1.0 H₂O (%): C 53.77, H 3.41, N 7.10; found: C 53.99, H 3.72, N 7.26.

^1H NMR (400 MHz, $\text{ACN-}d_3$): δ [ppm] 8.67-8.59 (2H), 8.55-8.46 (2H), 8.43-8.36 (1H), 8.32-7.93 (16H), 7.87-7.65 (4H), 7.56-7.46 (2H), 7.43-7.32 (2H), 7.07-6.93 (2H), 6.17-6.06(1H), 3.94-3.88(1H), 3.49-3.38 (2H), 2.40-2.32 (3H).

^1H NMR spectra of target complexes

The combination of the intrinsic chirality of ruthenium tris-diimine complexes and the chiral carbon atom in the backbone of racemic **bpy-pyrene** results in diastereomers with different NMR signals as displayed in Fig. S1. This can be easily visualized by the pseudo doublets of the CH_3 signals with ratios close to 1:1 (the CH_3 of the free **bpy-pyrene** ligand is a clear singlet) and the multiplets observed for CH . However, the occurrence of different isomers complicates the interpretation of both NMR spectra, especially in the overcrowded aromatic region (insets of Fig. S1).

We stress that such isomer effects were not observed during the photochemical investigations of both dyads indicating identical (photochemical) properties of their diastereomers.

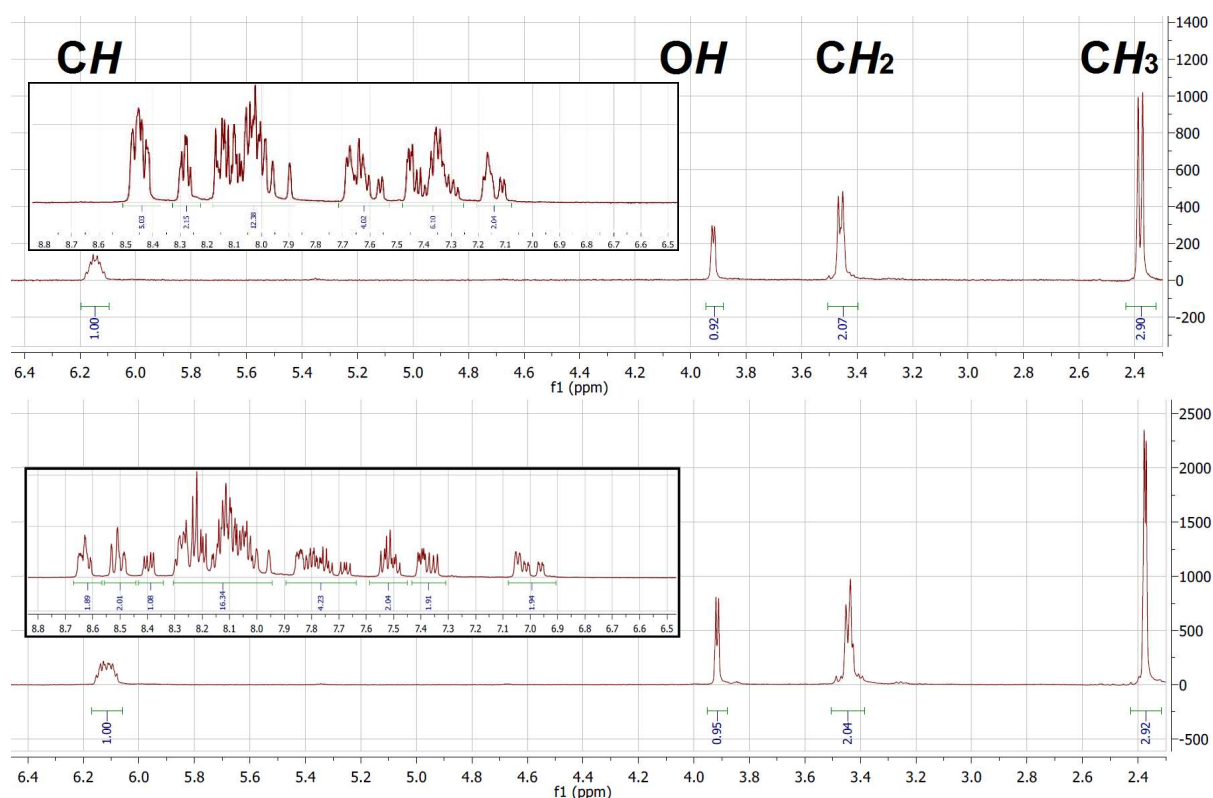


Fig. S1: Main plots, aliphatic and hydroxylic proton regions of the ^1H NMR spectra of **RuPy1** (top) and **RuPy2** (bottom) in $\text{ACN-}d_3$. Insets, signals of the corresponding aromatic protons. For further explanations, see text.

3 Rate constant determinations

3.1 Triplet-triplet energy transfer

The triplet-triplet energy transfer (TTET) between all energy donor/acceptor couples was investigated with time-resolved luminescence studies of the Ru-based sensitizers. At least four different concentrations of the anthracene acceptor were employed and the bimolecular rate-constants (k_{TTET}) were determined using the well-known Stern–Volmer equation. Fig. S2 illustrates two examples of that procedure (the other rate constants so obtained are given in Table 1 of the main paper). In all cases, purely dynamic quenching was observed and additional steady-state quenching experiments gave practically the same rate constants. Furthermore, the data presented in Fig. S2 show that the unquenched lifetime of $^3\text{Rubpy}$ does not depend on the pH value. The same pH-independence was observed for the dyads **RuPy1** and **RuPy2**.

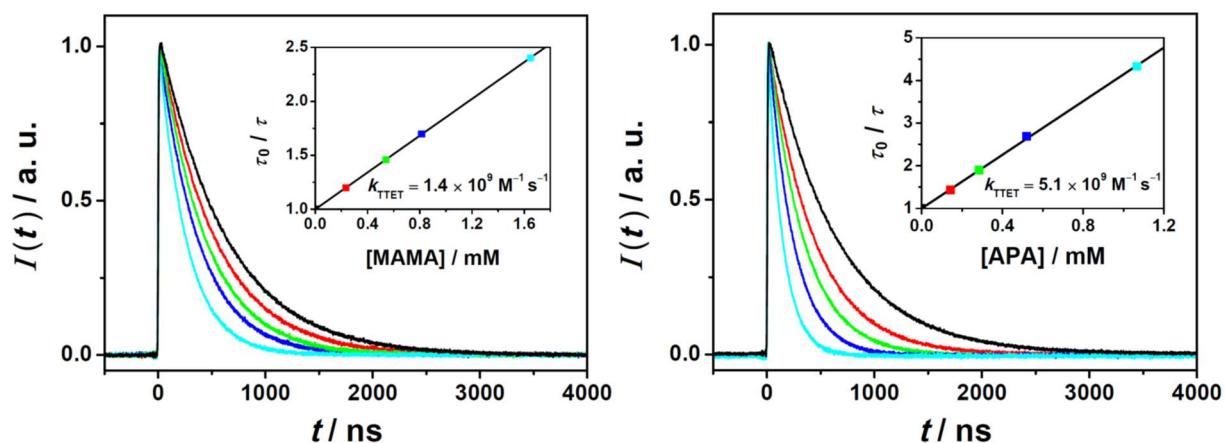


Fig. S2: Energy transfer from $^3\text{Rubpy}$ to **MAMA** (left) and **APA** (right) investigated by time-resolved measurements of the $^3\text{Rubpy}$ luminescence at 620 nm in Ar-saturated aqueous solutions (left, 33 μM **Rubpy** at pH 2; right, 30 μM **Rubpy** at pH 12) upon excitation with 532 nm laser pulses (37 mJ). The insets display the corresponding Stern–Volmer plots based on luminescence lifetimes using the same colour code for the concentrations as in the main plots.

3.2 Triplet-triplet annihilation

The triplet states of the anthracenes (^3M) decay with mixed first- and second-order kinetics under conditions suitable for triplet-triplet annihilation.^{1,9} To extract the rate constants of both processes, unquenched triplet decay (k_{T}) and triplet-triplet annihilation (k_{TTA}), from the concentration-proportional transient absorption signal (ΔA) of the respective ^3M , the data at different ^3M starting concentrations were fitted according to Eqn. S1. With the parameter β (Eqn. S2) and the initial ^3M concentration ($[^3\text{M}]_0$), which was obtained from the initial transient absorption using the molar absorption coefficients given in the main paper (Table 2), the kinetic constants can be calculated from each experimental trace.

$$\Delta A = \frac{\Delta A_0 \times (1 - \beta)}{\exp(k_T \times t) - \beta} \quad (S1)$$

$$\beta = \frac{k_{TTA} \times [{}^3M]_0}{k_{TTA} \times [{}^3M]_0 + k_T} \quad (S2)$$

The triplet decay analysis of both **APA** and **MAMA** was carried out by using different laser energies to vary $[{}^3M]_0$; the data range used for fitting was chosen such that the triplet-triplet energy transfer between **³Rubpy** and the acceptor/annihilator is already completed (an example is given in Fig. S3). Moreover, the initial **³MAMA** concentration was changed by using sensitizers with different lifetimes (see Fig. 5 (a) of the main paper). The kinetic parameters obtained from all decay analyses were averaged. The results for both anthracenes (together with standard deviations) are summarized in Table 2 of the main paper.

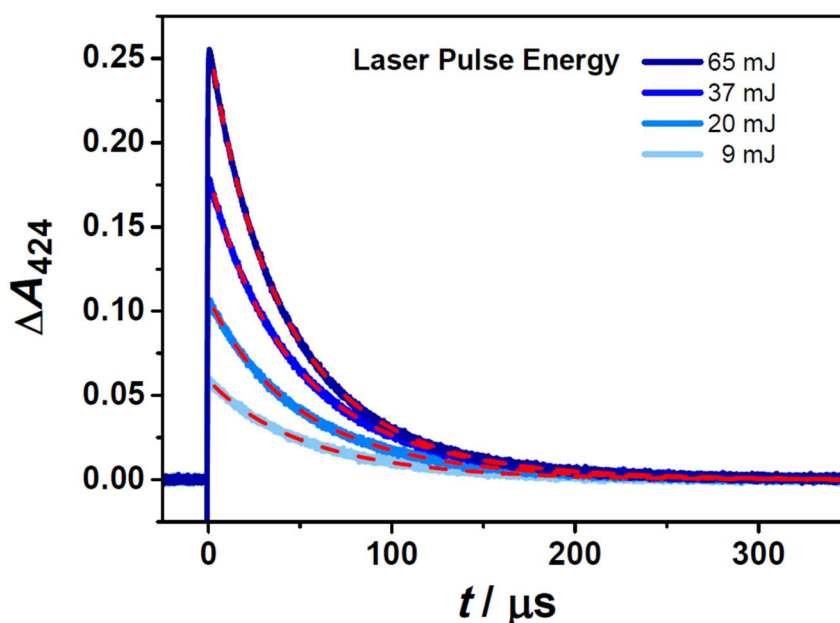


Fig. S3: Decay of **³APA** in Ar-saturated aqueous solution (30 μ M **Rubpy**, 0.52 mM **APA**, pH 12) following excitation at 532 nm with laser pulses of different energies and triplet-triplet energy transfer from **³Rubpy** to **APA**. The experimental traces at 424 nm are overlaid with the best-fit functions given by Eqn. S1. For further explanations, see text.

4 Control experiments with anthracene-9-propionate **APA**

Fig. S4 turns to the delayed luminescence when **APA** is employed as acceptor/annihilator. The luminescence spectra show the characteristic monomer fluorescence and an additional band centered at 530 nm, with the latter being characteristic for the anthracene excimer fluorescence¹⁰. All spectra recorded at different **APA** concentrations are practical identical, except for a filter effect in the absorption/fluorescence overlap region of **APA** (below 410 nm). Moreover, the luminescence kinetics of both build-up and decay are identical at 414

nm (maximum of monomer fluorescence) as well as 530 nm (maximum of excimer fluorescence) under the “upconversion” conditions of Fig. S4.

To understand that constant but unusual monomer-to-excimer emission ratio, we first studied the concentration dependence of the UV-Vis absorption spectrum of **APA**. In the concentration range used ($10 \mu\text{M} \leq [\text{APA}] \leq 0.4 \text{ mM}$), we did not detect any deviation from the Beer–Lambert law. Having excluded ground-state aggregation by these experiments, we next carried out concentration dependent fluorescence measurements after direct excitation of **APA**. At **APA** concentrations as high as 5 mM, the steady-state fluorescence spectrum does not contain the signature of the excimer (Ar-saturated solution), which rules out the **APA** excimer formation under conditions of prompt emission. However, the **APA** fluorescence lifetime of that solution decreases by 12 % (compared to that measured with strongly diluted solutions). We attribute that effect to self-quenching, *i.e.*, the reaction between singlet-excited **APA** and ground-state **APA**. Furthermore, the presence of **Rubpy** at a concentration identical to that used in Fig. S4 does neither change the excited-state lifetime nor the emission spectrum of **APA** upon direct excitation of the anthracene.

All these findings are in accordance with a dual emission caused by the unique geometry of the TTA encounter complex between **Rubpy** and **APA** (which does not occur when **ACA** or **MAMA** are used as annihilator). This conclusion is also substantiated by a previous study on the TTA process of several pyrene derivatives¹¹.

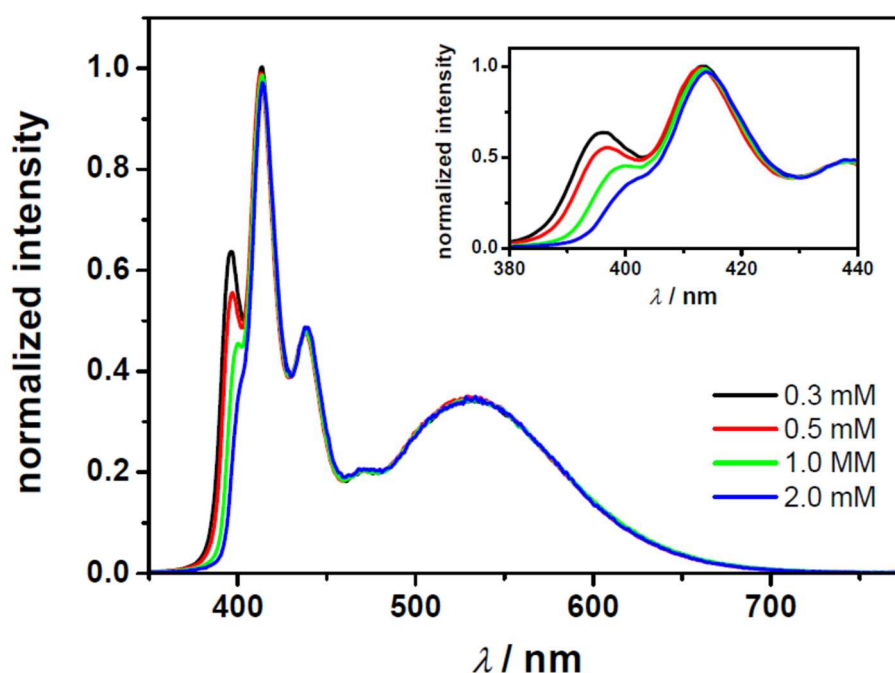


Fig. S4: Influence of the **APA** concentration on the delayed luminescence in the system **Rubpy** (30 μM) / **APA** (concentrations given in the figure) upon green-light excitation (532 nm, 40 mJ) of an Ar-saturated aqueous solution at pH 12. Main plot, time-integrated (over 400 μs starting immediately after the decay of $^3\text{Rubpy}$) emission spectra. Inset, data from the main plot on enlarged scale showing the filter effect caused by high **APA** concentrations. All spectra have been normalized using the peak at 438 nm, where **APA**-derived filter effects are absent. For further information, see text.

5 Upconversion quantum yield estimation

In order to estimate the upconversion quantum yield (ϕ_{UC}) of our improved system (**RuPy2** / **MAMA**), we analyzed the complete emission profile. To this end, we first measured the emission spectrum with our LFP setup with an integration time long enough to detect both the (quenched) luminescence of the sensitizer and the complete upconverted fluorescence of the acceptor (blue spectrum in Fig. S5). We then recorded a spectrum of the pure delayed fluorescence of excited **MAMA** by starting the time integration after the decay of excited **RuPy2** (10 μ s delay) with all other experimental parameters unmodified, and also measured the emission in the absence of **MAMA** to detect the luminescence of the sensitizer independently. Scaling of these spectra at their respective maximum to that of the blue spectrum is straightforward as shown in Fig. S5. Not only does that procedure provide a reliable spectral separation, but it also allows the removal of laser scattering light from the initial spectrum.

From the known rate constant of TTET in that system and the unquenched lifetime of excited **RuPy2**, the efficiency of TTET at the quencher concentration used ($[MAMA] = 0.25$ mM) is calculated to be 0.914; in other words, the apparent luminescence quantum yield of **RuPy2** under these conditions is $(1 - 0.914)$ times ϕ_{em} (see Table 1 of the main paper). The remaining **RuPy2** emission in Fig. S5 thus serves as internal reference with a quantum yield of $\phi_{Ref} = 0.84$ %. We regard that internal reference signal as very reliable because it avoids uncertainties associated with relative actinometry using external laser measurements (*e.g.* excitation intensities). To minimize systematic errors that result from the comparison of poorly overlapping emission spectra, we finally converted the signatures of both emitting species to the wavenumber scale (inset of Fig. S5) thereby eliminating the underestimation (about 50 %) of the relative **MAMA** fluorescence owing to the non-linear nature of the wavelength scale. The integrals I of the spectra so obtained were directly used for the quantum yield estimation (I_{UC} for upconverted fluorescence, I_{Ref} for 3RuPy2 emission).

For calculating ϕ_{UC} , we used the equation from ref. ⁹, which takes into account that at least two absorption processes are required for one upconverted photon allowing a theoretical ϕ_{UC} maximum of 100 %. That equation simplifies to give Eqn. (S3), since the initial absorbance associated with reference and upconverted emission is identical in our case.

$$\phi_{UC} = 2 \times \phi_{Ref} \times (I_{UC} / I_{Ref}) \quad (S3)$$

The resulting upconversion quantum yield, 0.90 %, is one order of magnitude higher than the estimated limit in the first TTA upconversion study in pure water¹². Additional fluorescence lifetime measurements at the **MAMA** concentration used in the upconversion experiments gave the same value as in strongly diluted solutions, indicating that self-quenching does not play any role under our conditions. For the discussion of the quantum yield, see Section 2.3 of the main paper.

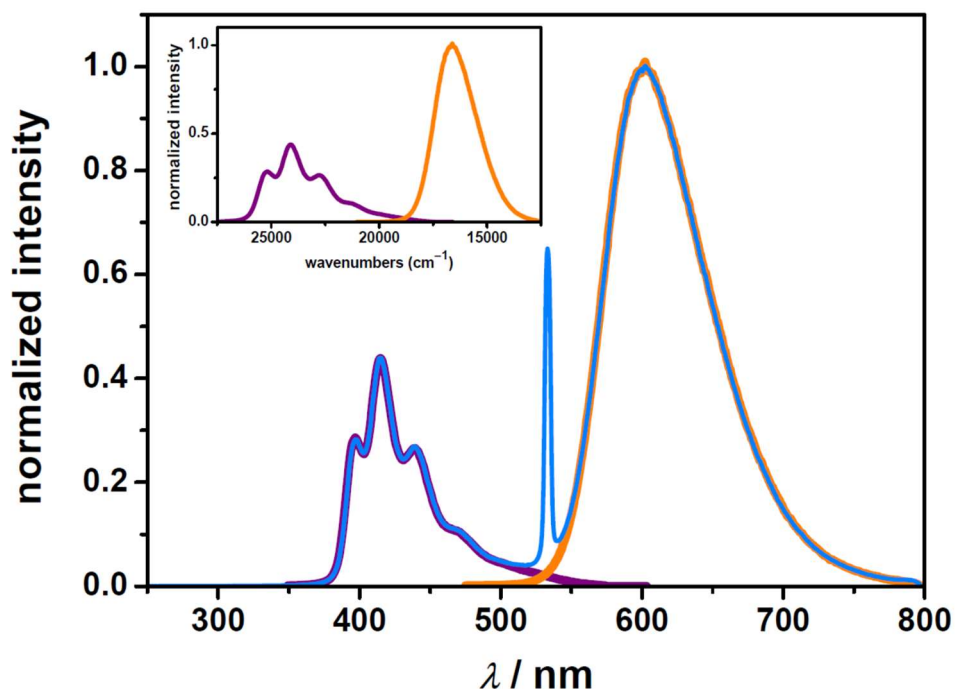


Fig. S5: Upconversion quantum yield estimation for the system **RuPy2** (28 μM) / **MAMA** (0.25 mM) upon green-light excitation (532 nm; laser pulse energy, 37 mJ). Main plot, time-integrated (over 400 μs starting with the laser pulse) emission spectrum (blue) and its separation into upconverted **MAMA** fluorescence (violet) and remaining MLCT luminescence of the sensitizer **RuPy2** (orange). The peak at 532 nm is due to stray light of the excitation source. Inset, upconverted emission (violet) and the reference signal (orange), which were converted to the wavenumber scale. The integrals of these signals were directly used for the quantum yield estimation. For further information, see text.

6 Applicability of the new dyads as oxygen probes

Fig. S6 displays the effect of dissolved oxygen on the steady-state luminescence spectra of the ruthenium complexes under study. To quantify their sensitivity for oxygen sensing, the parameter $I_{\text{Ar}} / I_{\text{air}}$ (compare, Fig. S6) was calculated for each complex. The respective substance-specific parameter is practically identical regardless of whether it is based on integrated luminescence spectra or on (monoexponential) luminescence lifetimes, which are also given in Fig. S6.

In addition to the sensitivity parameter comparing the luminescence intensities of the respective probe in aqueous solution saturated with inert gas (I_0 or I_{Ar}) and saturated with air (I_{air}), the quantum yield of the unquenched emission (ϕ_{em}) represents another important application-related quantity. These data, together with the unquenched luminescence lifetimes as well as the Stern–Volmer constants for oxygen quenching, are summarized in Table S1 and compared to those of known Ru-based oxygen probes in aqueous media (see also the corresponding discussion in Section 2.1 of the main paper). The table entries of the three compounds possessing the highest emission quantum yields and sensitivity parameters have been highlighted, clearly illustrating the advantage of using the dyad **RuPy2**.

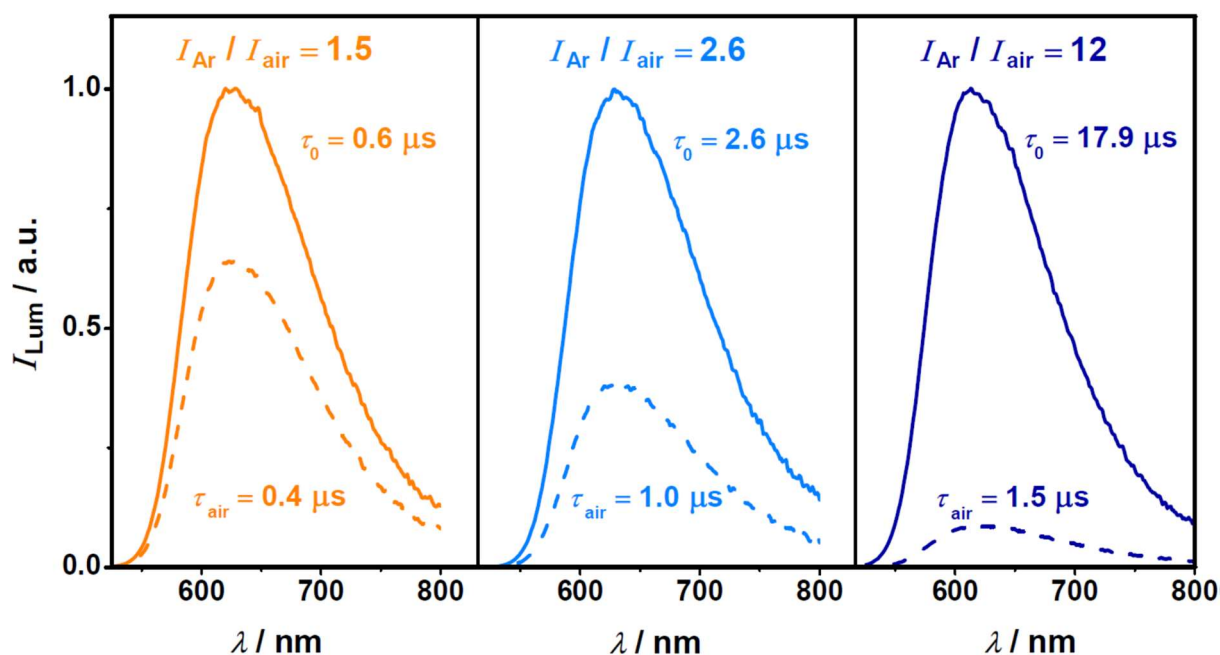


Fig. S6: Luminescence spectra of **Rubpy** (left) and the new dyads (**RuPy1**, center; **RuPy2**, right) in the absence of dissolved oxygen (solid lines) and in air-saturated water (dashed lines), respectively. For further details, see text.

Table S1: Photochemical properties relevant for oxygen sensing of already existing Ru-based oxygen probes and of our new dyads (**RuPy1** and **RuPy2**).

Compound	$\tau_0 / \mu\text{s}^{[a]}$	$\phi_{\text{em}}^{[b]}$	$K_{\text{SV}} / \text{M}^{-1}[c]$	$I_0 / I_{\text{air}}^{[d]}$
Rubpy ^{13 [e]}	0.60	0.063 ³	1850	1.5
[Ru(phen)₃]²⁺ ¹⁴	0.96	0.058	4060	2.1
Ru-NI 1 ¹⁵	0.67	0.021	2200	1.5
Ru-NI 2 ¹⁵	0.55	0.005	1720	1.4
Ru[dpp(SO₃)₂]₃⁴⁻ ¹⁶	3.7	n.d. ^[f]	11330	4.0
Ru-Py ¹⁷	17.5	0.031	10350	3.8
Ru-NMe₂ ¹⁷	4.5	0.045	2300	1.6
Ru-alkyl ¹⁷	3.2	0.050	2990	1.8
Ru-Cou 1 ¹⁸	n.d. ^[f]	0.111	7530	2.5 ^[g]
RuPy1 ^[e]	2.6	0.058	5970	2.6
RuPy2 ^[e]	17.9	0.098	42020	12.3

[a] Unquenched lifetime of the emissive excited state in homogeneous aqueous solution at room temperature. [b] Emission quantum yield under the conditions as in [a]. [c] Stern–Volmer constant for the reaction of the emissive state with dissolved oxygen. [d] Ratio of the integrated fluorescence of the respective probe in the absence of dissolved oxygen and in air-saturated solution (0.27 mM of dissolved oxygen)¹⁴. [e] This work. [f] Not determined. [g] Extracted from Fig. 2 of ref. ¹⁸.

7 Monodechlorination of trichloroacetate TCA⁻

To investigate the quenching of the singlet-excited anthracenes *Ant⁻ with TCA⁻, which should occur through an electron transfer from *Ant⁻ to TCA⁻ followed by instantaneous dissociation of the latter into a chloride ion and a dichloroacetate radical (see Section 2.4 of the main paper and ref. ¹⁹), we used TCSPC and scrutinized the effect of TCA⁻ on the excited-state lifetimes of the three anthracene derivatives under study. Following direct excitation of **MAMA** and **APA**, dynamic quenching was observed as indicated by the linear lifetime-based Stern–Volmer plots (an example is given in Fig. S7), whereas for **ACA** we did not even observe any quenching at our highest TCA⁻ concentration (50 mM) employed. The measurements with **MAMA** were carried out at pH 3.0 (compare, Section S1) to ensure that TCA⁻ is exclusively (> 99 %) present in its ionic form (the pK_a of trichloroacetic acid is about 0.5)¹⁹.

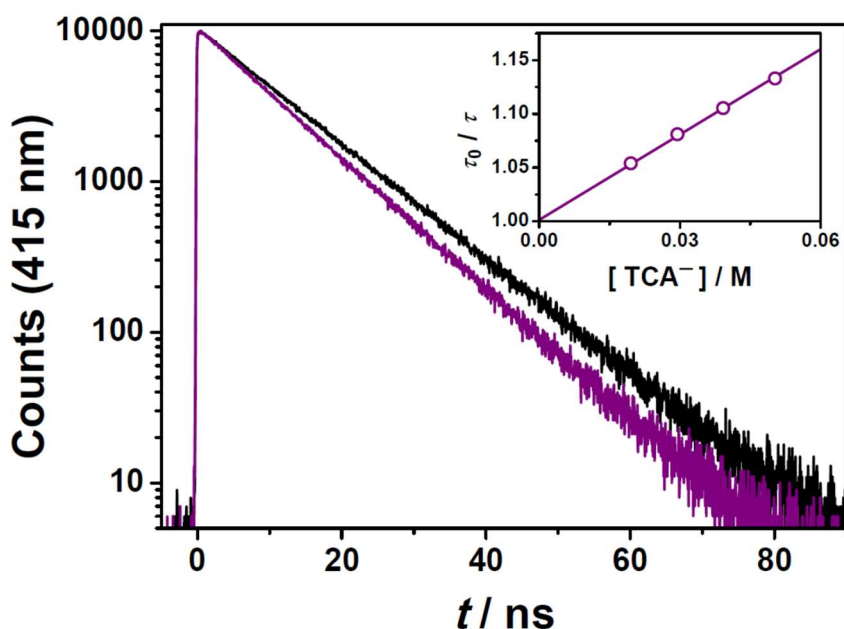


Fig. S7: Main plot, luminescence decay of **MAMA** in the absence of TCA⁻ (black trace) and with 55 mM TCA⁻ (violet trace) after 375 nm excitation of an argon-saturated aqueous solution (50 μ M **MAMA**, pH 3.0). Inset, corresponding Stern–Volmer plot. For further information, see text.

However, taking into account the rather short lifetime of singlet-excited **ACA**, we estimated an upper limit for the quenching rate constant, which is, together with the results obtained for the other anthracenes, summarized in Table S2. Moreover, the calculated quenching efficiencies assuming a synthetically useful TCA⁻ concentration (10 mM) are included in that table.

Table S2: Oxidative quenching of singlet-excited anthracene derivatives with the electron acceptor trichloroacetate TCA^- .

Anthracene	τ_0 (S_1) / ns ^[a]	k_{TCA^-} / ($\text{M}^{-1} \text{s}^{-1}$) ^[b]	η_q (10 mM) ^[c]
ACA	1.3	$< 1 \times 10^8$	$< 0.1 \%$
APA	10.9	8.0×10^8	8.0 %
MAMA	11.3	2.3×10^8	2.5 %

[a] Unquenched lifetime of the excited singlet state. [b] Rate constant for the reaction between singlet-excited anthracene and trichloroacetate TCA^- . [c] Calculated efficiency of oxidative quenching at a TCA^- concentration of 10 mM.

Recently, a chloride-sensitive electrode has proven very useful for studying a similar dechlorination in aqueous solution.²⁰ This prompted us to carry out several irradiation experiments with the most reactive anthracene (**APA**, see Table S2) in the presence of TCA^- , combined with subsequent measurements of the chloride ion concentrations. For the chloride measurements, 2.5 mL of the solutions with unknown Cl^- concentration were diluted to 4.5 mL, 1 mL ionic strength adjuster (solution provided by the electrode manufacturer) was added and the pH was adjusted to 4 with an acetate buffer (1 mL, 1 M). The potentials of these solutions were measured with a HI4107 electrode (Hanna Instruments) following the instructions given by the manufacturer. Calibration of the electrode with solutions containing well-defined Cl^- concentrations was carried out directly before each series of measurements. A typical calibration curve is shown in Fig. S8.

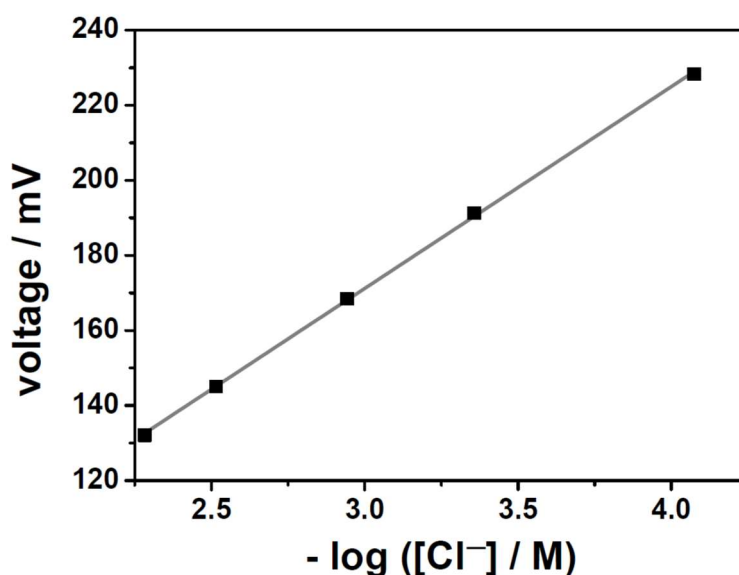


Fig. S8: Typical calibration curve of the HI 4107 electrode. The linear regression line was used for chloride ion determination (expected errors < 0.1 mM). Calibration measurements and the determinations of unknown chloride concentrations were carried out at the same ionic strength and pH. For further details, see text.

All irradiation experiments were carried out in fluorescence cuvettes (1 cm \times 1 cm \times 4 cm) under continuous stirring using either a 405 nm (optical power, 870 mW; full width at half

maximum, 19 nm) collimated LED (Thorlabs) or a 532 nm (optical output, 500 mW) DPSS cw laser (Roithner Lasertechnik) as light source. The LED was adjusted such that the whole solution was irradiated, whereas the cw laser was collimated to a diameter of 2 mm to achieve intensities high enough for efficient sensitized TTA. Since only the short-wavelength emission edge of the LED overlaps with the absorption of **APA**, we use the term “ $\lambda < 400$ nm” when referring to irradiation with that light source.

For all irradiation experiments, 10 mL of the respective solution were prepared; an aliquot of 3 mL was used for photoirradiation and the blank chloride concentration (mainly caused by impurities in the sodium salt of TCA⁻ (TCANa) and the chloride counterions of **Rubpy**) was carefully determined with the remaining solution. The results of all irradiation and control experiments have been compiled in Table S3.

Table S3: Laboratory-scale dechlorination of TCA⁻.^[a]

Entry	[TCANa] / mM	[APA] / mM	[Rubpy] / mM	Conditions ^[b]	(Mono)Dechlorination / % (mM) ^[c]
1	10	10	–	405 nm LED, 2 h, Ar	75 % (7.5)
2	10	10	–	no irradiation, 2 h, ^[d] air	0 % (0.0)
3	20	–	–	405 nm LED, 2 h, Ar	0 % (0.05)
4	20	10	–	405 nm LED, 2 h, Ar	48 % (9.5)
5	10	10	–	405 nm LED, 2 h, air	70 % (7.0)
6	10	12	–	405 nm LED, 2 h, air	81 % (8.1)
7	20	10	0.25	532 nm cw laser, 3 h, Ar	25 % (5.0)
8	20	10	0.25	532 nm cw laser, 3 h, air	24 % (4.7)
9	20	10	0.25	no irradiation, 3 h, ^[d] air	0 % (0.0)
10	20	10	–	532 nm cw laser, 3 h, air	< 1 % (0.1)
11	20	–	0.25	532 nm cw laser, 3 h, air	1 % (0.15)
12	10	12	0.25	532 nm cw laser, 3 h, air	38 % (3.8)
13	10	12	0.5	532 nm cw laser, 3 h, air	43 % (4.3)

[a] Carried out at room temperature in homogeneous aqueous solutions containing 20 mM of NaOH. [b] Light source, reaction time and gas/gas mixture dissolved in the solution. [c] Determined from the chloride concentration in the solution measured using a chloride sensitive electrode. For details, see text. [d] Solutions stored in the lab under “daylight conditions”, but without an additional light source.

Given the fact that the activation of TCA⁻ by singlet-excited **APA** is slower than the diffusion limit by one order of magnitude (Table S2), we expect the reaction of the latter with the less activated dichloroacetate fragments produced in the course of photoirradiation to be too slow to play any role under our conditions. The same holds true for a complete dechlorination of the starting material because the dissociative electron transfer to the model compound chloroacetate²⁰ would require about 1 V more reductive power than ¹**APA*** can provide (see Section 2.4 of the main paper). Hence, the only source of chloride ions in the reactions presented in Table S3 is the monodechlorination of TCA⁻.

In line with the observation that dissolved oxygen has only a minor effect on the product yields of our photoreactions, we observed a substantial increase of the oxygen-sensitive ^3APA lifetime upon irradiation of an air-saturated solution (Fig. S9). These results clearly indicate an efficient oxygen-scavenging pathway in our system, allowing photochemical reactions without oxygen removal. For a discussion of that effect, see the main paper.

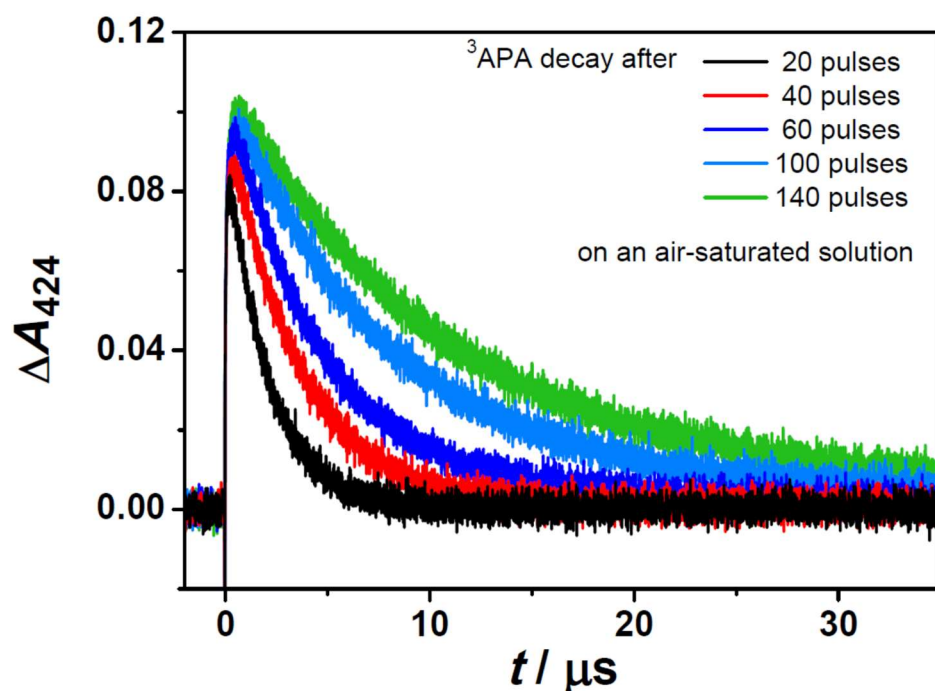


Fig. S9: Oxygen removal from an air-saturated aqueous solution (25 μM **Rubpy**, 5 mM **APA**, 20 mM NaOH) visualized by monitoring the lifetime of ^3APA at its absorption maximum after different numbers of laser pulses on the same sample. ^3APA was indirectly generated after excitation of **Rubpy** with green laser pulses (532 nm, 15 mJ pulse energy) and subsequent energy transfer. For further explanations, see text.

Exploiting the long-lived excited dyads as sensitizers for the reductive dechlorination

To test whether sensitizers with long-lived excited states have also a beneficial effect on the reductive TCA^- dechlorination, we used **MAMA** at a standard concentration as low as 1 mM and performed irradiation experiments in the presence of excess TCA^- . A significantly higher TCA^- concentration (30 mM) was necessary to overcompensate the lower kinetic reactivity of excited **MAMA** relative to **APA** (compare, Table S2). High blank chloride ion concentrations were avoided by using phosphate-buffered solutions instead of solutions acidified with hydrochloric acid. The UV-Vis absorption and fluorescence lifetime (Fig. S10) properties of the anthracene derivative **MAMA** at pH 7.8 are identical to those observed in acidic solutions, indicating that **MAMA** exists exclusively in its protonated form at that pH. Contrary to the chloride ion determinations presented in Table S3, we used 2.5 mL of the solutions with unknown $[\text{Cl}^-]$, added 1.0 mL acetate buffer and 0.5 mL ionic strength adjuster. Calibration of the electrode was carried out as presented in the preceding section.

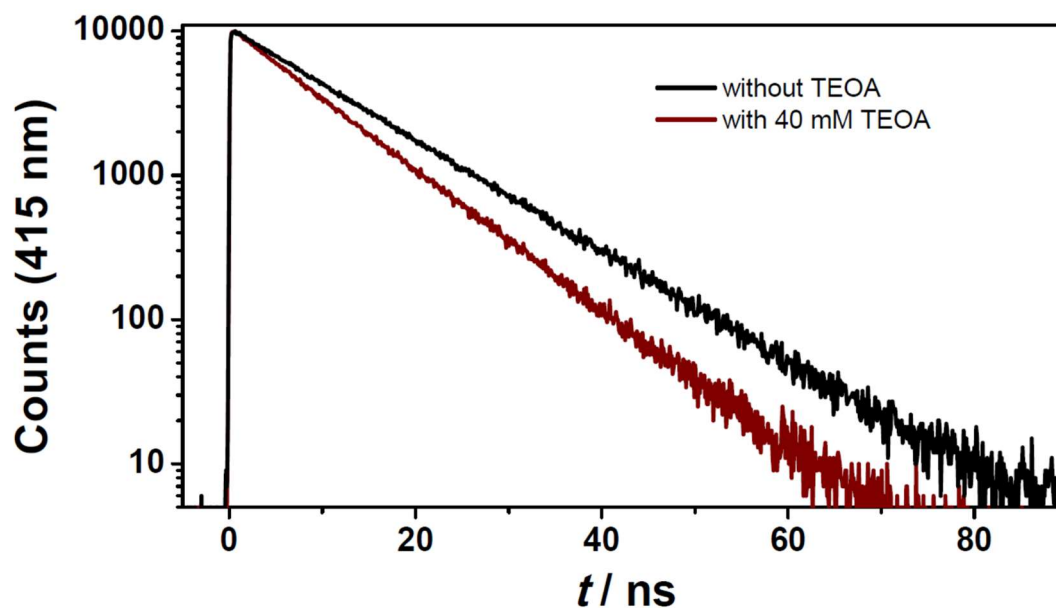


Fig. S10: Luminescence decay of **MAMA** in the absence of TEOA (black trace) and with 40 mM TEOA (red trace) after 375 nm excitation of argon-saturated aqueous solutions (45 μ M **MAMA**, pH 7.8). Monoexponential fits to the data gave lifetimes of 11.2 and 8.8 ns, respectively.

Upon irradiation with a 405 nm LED, we observed practically the same concentration of liberated chloride ions as initial **MAMA** used (Table S4, entry 1), indicating that these experimental conditions provide a good starting point for further investigations. In the presence of triethanolamine (TEOA), which should be able to regenerate the anthracene radical cation of **MAMA** produced by the photoreaction with TCA^- ,²¹ we did not observe the expected superincrease of the dechlorination efficiency (entry 2). We attribute the absence of catalytic activity to an unfavorable combination of a slow rate constant for the singlet-excited **MAMA** quenching by TCA^- and a fast deactivation of the **MAMA**-derived radical cation through a nucleophilic attack²² by TCA^- (which competes with the **MAMA** regeneration by TEOA). Moreover, in control experiments we observed **MAMA** fluorescence quenching with an efficiency of about 20 % (Fig. S10) under the same conditions as in entry 2 of Table S4. That lifetime decrease is most likely due to reductive quenching of singlet-excited **MAMA**, which is thermodynamically feasible¹⁴. The presence of the anthracene radical anion that would result from the quenching of excited **MAMA** with TEOA seems to play only a minor role under our conditions.

Table S4: Dechlorination of TCA⁻ using MAMA.^[a]

Entry	[MAMA] / mM	[Additive] / mM	[Sensitizer] / μ M	Conditions ^[b]	Dechlorination / mM ^[c]
1	1	–	–	405 nm LED, 30 min	0.95
2	1	40 (TEOA) ^[d]	–	405 nm LED, 30 min	1.05
3	1	–	–	447 nm cw laser, 10 min ^[e]	0.10
4	1	–	30 (Rubpy)	447 nm cw laser, 10 min ^[e]	0.25
5	1	–	25 (RuPy2)	447 nm cw laser, 10 min ^[e]	0.80

[a] Carried out at room temperature in Ar-saturated homogeneous aqueous solutions containing 40 mM of phosphate buffer at pH 7. [b] Light source and reaction time. 2.6 mL aliquots were used for photoirradiation. [c] Determined from the chloride concentration in the solution measured using a chloride sensitive electrode. [d] Carried out at pH 7.8 (*i.e.*, at the pK_a value of protonated TEOA) to keep half of the amine TEOA in its neutral (reactive) form. [e] Optical output of the cw laser, 500 mW. Beam diameter, 2 mm. For details, see text.

We next tried to compare the dechlorination efficiencies via the sensitized TTA mechanism using conventional **Rubpy** and our dyad with the longest excited-state lifetime, **RuPy2**. However, for solubility reasons, we could not use as high sensitizer concentrations as employed in the dechlorinations with the **Rubpy** / **APA** system (see, Table S3). In order to find conditions suitable for the preparative-scale TCA⁻ dechlorination, we tested a 447 nm (optical output, up to 1000 mW) diode laser (Roithner Lasertechnik) as light source. This cw laser produces almost monochromatic light (Fig. S11), its emission does not overlap with the ground-state absorption spectrum of **MAMA**, and perfectly matches the visible absorption maximum of the sensitizers thus allowing efficient and selective excitation at low sensitizer concentrations. Using that light source, we observed significant chloride concentrations in the presence of the two sensitizers (entries 4 and 5; different sensitizer concentrations were employed to ensure identical excitation conditions), whereas a control experiment (entry 3) gave almost no detectable chloride ions. For further discussions of the results presented in Table S4, see Section 2.4 of the main paper.

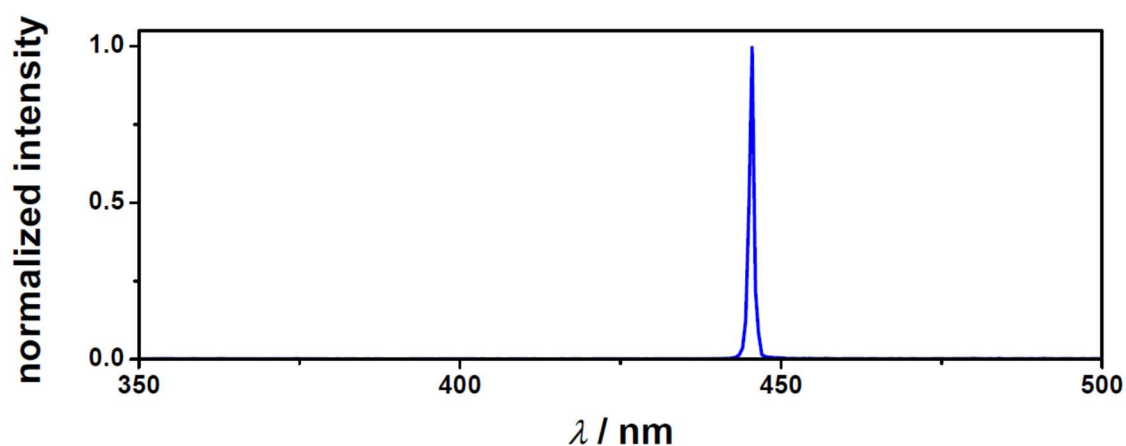


Fig. S11: Output spectrum of the RLMDL-447 diode laser measured with our fluorescence spectrometer (Fluorolog-3-22). The full width at half maximum is about 1 nm.

8 Supplementary references

- 1 K. A. El Roz and F. N. Castellano, *Chem. Commun.*, 2017, **53**, 11705–11708.
- 2 O. Johansen, A. W.-H. Mau and W. H. F. Sasse, *Chem. Phys. Lett.*, 1983, **94**, 107–112.
- 3 K. Suzuki, A. Kobayashi, S. Kaneko, K. Takehira, T. Yoshihara, H. Ishida, Y. Shiina, S. Oishi and S. Tobita, *Phys. Chem. Chem. Phys.*, 2009, **11**, 9850–9860.
- 4 H. E. Gottlieb, V. Kotlyar and A. Nudelman, *J. Org. Chem.*, 1997, **62**, 7512–7515.
- 5 B. P. Sullivan, D. J. Salmon and T. J. Meyer, *Inorg. Chem.*, 1978, **17**, 3334–3341.
- 6 L.-Y. Zhang, Y.-J. Hou, M. Pan, L. Chen, Y.-X. Zhu, S.-Y. Yin, G. Shao and C.-Y. Su, *Dalton Trans.*, 2015, **44**, 15212–15219.
- 7 S. Thota, S. Vallala, M. Imran, S. Mekala, S. S. Anchuri, S. S. Karki, R. Yerra, J. Balzarini and E. De Clercq, *J. Coord. Chem.*, 2013, **66**, 1031–1045.
- 8 D. S. Tyson and F. N. Castellano, *J. Phys. Chem. A*, 1999, **103**, 10955–10960.
- 9 T. N. Singh-Rachford and F. N. Castellano, *Coord. Chem. Rev.*, 2010, **254**, 2560–2573.
- 10 T. N. Singh-Rachford, R. R. Islangulov and F. N. Castellano, *J. Phys. Chem. A*, 2008, **112**, 3906–3910.
- 11 C. Bohne, E. B. Abuin and J. C. Scaiano, *J. Am. Chem. Soc.*, 1990, **112**, 4226–4231.
- 12 K. El Roz, *PhD thesis*, North Carolina State University, 2017.
- 13 K. J. Morris, M. S. Roach, W. Xu, J. N. Demas and B. A. DeGraff, *Anal. Chem.*, 2007, **79**, 9310–9314.
- 14 M. Montalti, A. Credi, L. Prodi and M. T. Gandolfi, *Handbook of photochemistry*, CRC/Taylor & Francis, Boca Raton, 3rd ed., 2006.
- 15 A. Son, A. Kawasaki, D. Hara, T. Ito and K. Tanabe, *Chem. Eur. J.*, 2015, **21**, 2527–2536.
- 16 F. N. Castellano and J. R. Lakowicz, *Photochem. Photobiol.*, 1998, **67**, 179–183.
- 17 H. Komatsu, K. Yoshihara, H. Yamada, Y. Kimura, A. Son, S. Nishimoto and K. Tanabe, *Chem. Eur. J.*, 2013, **19**, 1971–1977.
- 18 D. Hara, H. Komatsu, A. Son, S. Nishimoto and K. Tanabe, *Bioconjug. Chem.*, 2015, **26**, 645–649.
- 19 X. Liu, J. Zhong, L. Fang, L. Wang, M. Ye, Y. Shao, J. Li and T. Zhang, *Chem. Eng. J.*, 2016, **303**, 56–63.
- 20 T. Kohlmann, R. Naumann, C. Kerzig and M. Goetz, *Photochem. Photobiol. Sci.*, 2017, **16**, 1613–1622.
- 21 M. S. Workentin, L. J. Johnston, D. D. M. Wayner and V. D. Parker, *J. Am. Chem. Soc.*, 1994, **116**, 8279–8287.
- 22 M. Schmittel and A. Burghart, *Angew. Chem. Int. Ed.*, 1997, **36**, 2550–2589.